Journal of Materials Chemistry B

Accepted Manuscript

ROYAL SOCIETY OF CHEMISTRY

www.rsc.org/materialsB

Journal Name Journal of Materials Chemistry B Dynamic Article Links ►

Cite this: DOI: 10.1039/c0xx00000x

www.rsc.org/xxxxxx

ARTICLE TYPE

Rational design of NAMI-A-loaded mesoporous silica nanoparticles as antiangiogeneic nanosystem

Hao Hu, Yuanyuan You, Lizhen He, Tianfeng Chen*

Received (in XXX, XXX) Xth XXXXXXXXX 20XX, Accepted Xth XXXXXXXXX 20XX
DOI: 10.1039/b000000x

Angiogenesis is essential for tumorous progression and metastasis. The RGD (Arg-Gly-Asp acid) peptide has been demonstrated as a remarkable targeting reagent and can be distinguished by integrin receptor overexpressed in various human tumor cells. Mesoporous silica nanoparticles (MSNs) is one of the most applied promising carriers for delivery drugs or genes. It is well-known that NAMI-A is an excellent drug for ant-migration of tumor cells. Targeting tumor vasculature with RGD-modified nanomaterials were expected as a promising strategy for cancer therapy. Herein we investigated the antiangiogenic activity of NAMI-A-loaded and RGD peptide surface decorated mesoporous silica nanoparticles *in vitro* and *in vivo*. The results revealed that, NAMI-A@MSN-RGD remarkably enhanced the cellular uptake and antiangiogenic efficacy in contrast to bare NAMI-A *in vitro*. The nanosystem of NAMI-A@MSN-RGD exhibited also inspiring antiangiogenic action in vivo assay. Furthermore, RGD-functionalized nanodrug inhibited angiogenesis by means of apoptosis through trigging ROS-mediated DNA damage in human umbilical vein endothelial cells (HUVECs). Our results suggested that the use of RGD-peptide modified MSNs as a vehicle of anticancer drugs is an efficient way to construct cancer-targeted nanosystem with antiangiogenic activity.

1 Introduction

Angiogenesis, expanding of the endothelium and formation of new blood vessels, plays significant roles in carcinogenesis, cancer progression and metastasis, which will lead to the augmentation of solid tumors.[1-3] Tumor angiogenesis can supply necessary nutriments and oxygen to the tumor microenvironment, which urges the transformation of small, dormant cancers into invasive and metastatic forms.[4, 5] Therefore, the inhibition of angiogenesis is expected to be a favorable therapeutic method for cancer. For example, Garcia-Vilas *et al.* demonstrated the outstanding antiangiogenesis of 4-methylumbelliferone *in vitro* and *in vivo*.[6] Aaron also described the new analogues of motuporamines which exhibit doubled antimigration potency and reduced cytotoxicity.[7] Therefore, Creation and conformation of a new effective anti-angiogenic drug or system is still a meaningful task.

Ruthenium-based complexes have recently attracted an increased attention as the next generation of metal-based substitute to Platinum-antitumor agents.[8-13] Some of them have achieved prodigious progress in pre-clinical phase and one of the most famous is the NAMI-A (imidazolium trans-imidazoledimethyl-sulfoxidetetrachlororutheate), which is now undergoing further clinical investigations.[14-17] These metal complexes usually present powerful cytotoxicity in antiangiogenesis. Most importantly, their cytotoxinic side effect can be ignored. However, in human clinical stage, intravenous injection of Ruthenium-based complexes usually led to widely binding to blood proteins during the blood circulation.[17-19] Such binding is considered to be adverse for the intracellular uptake of metal-based compounds, resulted the decline of anticancer activity.[20, 21] Therefore, the encapsulation of NAMI-A with nanoparticles are expected to be a rational and valid way to improve anti-angiogenic activity. Nano-phase materials exhibit noticeable performance in targeted drugs delivery, molecular diagnose and molecular imaging.[22-25] Among multifarious nanocarriers, for example polymeric nanoparticles, liposomes, protein particles, dendrimers and so on, mesoporous silica nanoparticles (MSNs) have been exactly demonstrated as an outstanding nanomaterial for drug delivery system,[26, 27] due to their unique physical and chemical properties including straightforward synthesis, large specific surface area and pore volume, regular pore channels, and capacious space to loading various drugs (complexes, macromolecular and other nanoparticles).[28-36] Moreover, silica was confirmed as "Generally Recognized As Safe" by the U.S. Food and Drug Administration

(FDA).[37] Liu *et al* created a new intelligent nanoplatform based on hollow mesoporous silica for targeted chemo-photothermal therapy. They used CuS nanoparticles for photothermal therapy and DOX for chemotherapy, which exhibited a powerful synergistic action.[38] Furthermore, targeted modification of MSNs could increase the recognition and internalization to cancer cells and avoid undesirable toxic side effect and improve efficiency of anticancer drugs.[39] So far, large numbers of targeted drugs have been exploited to modify the nanoparticles and have obtained great achievements, such as galactosamine, transferrin, folic acid, TAT, and RGD.[40, 41] The RGD (Arg-Gly-Asp acid) peptide could be identified by integrin receptor which is overexpressed in vascular endothelial cells and have attracted more and more interests.[42-45] Therefore, in this study, we have developed a new neovasculature-targeted drug delivery system depended on multifunctional MSNs which is modified with RGD peptide and loaded with NAMI-A. This system greatly enhanced the anti-angiogenesis activity and we roughly clarified the molecular mechanism demonstrated the positive action of NAMI-A@MSN-RGD.

2 Materials and methods

Materials

All reagents were used without further purification. Ethanol (CH3CH2OH), concentrated hydrochloric acid (HCl, 38%), dimethylsulfoxide (DMSO), acetone, diethyl ether and imidazole were analytically pure and were purchased from Baishi Chemical industry CO., LTD. (tianjin, china). Ruthenium (Ⅲ) chloride (RuCl3·3H2O, AR), tetraethylorthosilicate (TEOS,GR), hexadecyltrimethylammonium bromide (CTAB, 99%), N-hydroxysuccinimide (NHS), 1-ethyl-3-(3-dimethylaminopropyl) carbodiimide hydrochloride (EDC), triethanolamine (AR) and polyethyleneinimine (PEI, 99%) were purchased from Aladdin Chemistry Co., Ltd. cRGD (Arg-Gly-Asp) were purchased from Gier biochemistry CO., LTD. (shanghai, china).

Synthesis of NAMI-A@MSN-RGD

At first, NAMI-A complexes were synthesized according to the reported literature by little modification.[46] Mesoporous silica nanoparticles (MSNs) were synthesized by previously reports.[28, 40] In a typical procedure, 4.0 g CTAB were put into 40 ml distilled water and with ceaselessly stirring. After completely dissolution, 100 μL TEA (triethanolamine) were added to the solution and stirring another 2 h at 95℃. Next, 1.5 ml TEOS were slowly added into the settled solution and stirring about for 3 h further. The resulting white precipitate were gathered by centrifugation and then refluxed in HCL/methanol solutions overnight to washing off the residual CTAB. Finally, the nanoparticles were achieved by centrifugation and washed by ethanol and water five times respectively. After lyophilization, the targeted solid particles were gained.

To obtain the MSN-RGD particles, PEI-NH2 (Ethylene imine polymer, M.W. 600, 99%) was firstly reacted with the same amount of RGD (Arg-Gly-Asp) peptide by coupling reaction under EDC and NHS. After 12 h, the reaction mixtures were added into the suspension of MSNs, and then stirring overnight at room temperature .The suspension was centrifuged and then washed with water and ethanol five times respectively. The result solid particles were collected by centrifugation.

NAMI-A (10 mg) dissolved in 5 ml DMSO and then treated with an ultrasonic instrument for 2 minutes. Then 10 mg MSN-RGD nanoparticles were added into the NAMI-A solution and stirring overnight at ambient environment. Then finally particles were achieved by centrifugation and lyophilization.

Characterization of NAMI-A@MSN-RGD

The microstructure of NAMI-A@MSN-RGD was characterized by transmission electron microscopy (H-7650, Hitachi Co). The size distribution and zeta potential of nanoparticles were measured by a Nano-ZS instrument (Malvern Instrument Co). The characterization of mesoporous material was performed by a N2 adsorption-desorption method and the isotherms were recorded on a surface area analyzer (NOVOA, 4200e). The UV-vis spectroscopy (Carry 5000) was analyzed in the range of 200-800 nm.

Determination of NAMI-A and RGD

Concentration of NAMI-A was quantified by the determination of Ru with ICP-MS (Inductively coupled plasma mass spectrometry).[47] Bicinhoninic acid (BCA) kit was used to measure RGD peptide according to the literature.[45]

MTT Assay

The cytotoxic effect *in vitro* was investigated by MTT assay according to the literature.[48, 49] Briefly, The HUVECs were cultured in F-12 medium including 10 % fetal bovine serum, 1% penicillin and 0.01% streptomycin and cultivated in a CO2 incubator (95% relative humidity, 5% CO2, 37℃). Next, the cells (2×10^4 cells/ ml) were firstly seeded in a 96-wells plate for 24 h and then NAMI-A@MSN-RGD solutions were injected into the wells in different concentrations. After incubated for 72 h, 20 μl/well of the MTT solution was added and incubated for about 5 h at 37℃. Finally the medium was extracted and replaced with 200 μl DMSO per well, the plate was measured under a microplate spectrophotometer (SpectroAmaxTM250) at 570 nm.

In vitro cellular uptake of NAMI-A@MSN-RGD

The cellular uptake of NAMI-A@MSN-RGD and NAMI-A in HUVECs were quantitatively analyzed by ICP referring to the report.[50] In briefly, HUVECs (2×10^5 cells/ ml) were seeded into 10 cm dishes and allowed to incubating for 24 h. Then different concentrations of NAMI-A@MSN-RGD and NAMI-A were added and incubated for different periods of time. After completely absorption, the cells were collected with centrifugation and then washed off unabsorbed drugs with PBS. The content of intracellular Ru was tested with ICP-MS.

Flow cytometric analysis

The cell cycle distribution was analyzed by flow cytometry according to reported method.[50, 51] Briefly, cells (2×10^4 cells/ ml) were treated with NAMI-A@MSN-RGD at different concentrations for 72 h and then washed with PBS for three times, finally the cells were trypsinized and then fixed with 75% ethanol overnight at -20℃. The fixed cells were stained with propidium iodide (PI) for about 1 hour in darkness. At last the stained cells were measured with Epics XL-MCL flow cytometer (Beckman

Couler, Miami, FL) and Cell cycle distribution was analyzed with Multicycle software (Phoenix Flow Systems, San Diego, CA).The population of cells in G0/G1, S, and G2/M phases were expressed respectively as DNA histogram. Apoptotic cells with hypodiploid DNA content were expressed in the cell cycle pattern by quantifying the sub-G1 peak. For each experiment, 10,000 events per sample were recorded.

Real-time intracellular trafficking of NAMI-A@MSN-RGD

Real-time observation of intracellular localization of NAMI-A@MSN-RGD was monitored by fluorescence microscopy.[52] In brief, HUVECs (8×10^4 cells/ ml) were seeded in 2 cm culture dishes at a CO2 incubator for 24 h and then the fresh medium dissolved FITC@MSN-RGD were added into the dishes and incubated for 0-8 h in an CO2 incubator. Finally treated cells were stained with 1μL Lyso-Traker for lysosome, and 1μL DAPI for nucleuses. After half hour, the unstained cells were washed off by PBS and the stained cells were captured under fluorescence microscopy (IX51, Olympus).

***In vitro* drug release of NAMI-A@MSN-RGD**

Releasing of NAMI-A from MSN-RGD nanoparticles in different environments was investigated according to the literature.[45] Coumarin-6-loaded MSN-RGD (10 mg) was synthesized and then dispersed into PBS at pH 5.3, pH 7.4 and cell lysate respectively with constantly stirring at ambient temperature. Every 6 h, 200 ul of solution was extracted and 200 ul PBS or cell lysate were put in. The collected solution was centrifuged and the concentration of coumarin in supernate was measured under a fluorescence microscopy with excitation and emission wavelength set as 466 nm and 504 nm respectively.

RGD competing assay and endocytosis inhibitors blocking assay

The competing assay and blocking assay was performed according to the previously report.[53] Briefly, HUVECs (8×10^4 cells/ml) were seeded in a 96-well plate and allowed to growing for 24 h. The second day, HUVECs were pre-treated with RGD (0-2.5 mg/ml) for 2 h and then incubated with FITC labelled MSN-RGD (2 μM) for 6 h in a CO2 incubator, finally the cells were washed with PBS to remove the unabsorbed FITC@MSN-RGD and finaly read under a fluorescence microscopy. The RGD blocked the viability of HUVECs induced by NAMI-A@MSN-RGD was also performed with the similar method. At first, HUVECs were pretreated with RGD (2.5mg/ml) for 2 h and then incubated with NAMI-A@MSN-RGD for 24 h. The viability assay was analyzed by MTT. The endocytosis inhibitors blocked the cellular uptake of NAMI-A@MSN-RGD and improved the viability of HUVECs induced by NAMI-A@MSN-RGD were investigated in the same assay only replacing the RGD with endocytosis inhibitors.

***In vitro* migration**

HUVECs (2×10^5/ml) were seeded in a 6-well plate and allowed to growing to full confluence for 24 h.. After treated with medium F-12 medium containing 3% FBS for about 6 h, cells were wounded by pipette tips and washed with PBS for 3 times. The fresh F12 medium was added into every well, then VEGF (50 ng/ml) and various concentrations of NAMI-A@MSN-RGD were added. After incubated for enough times, migrated cells were photographed by using a digital camera (Olympus inverted microscope). The statistical analysis of migrated cells was analyzed by manual counting and inhibition of percentage was expressed using untreated cells as 100%. Three independent experiments were performed.

***In vitro* invasion assay**

Effects of NAMI-A@MSN-RGD on invasion of HUVECs were detected by Transwell. Boyden chamber (8 μm pore, Corning, Lowel, MA) were pre-coated with matrigel for 4 h at 37 ℃. 100 μl HUVECs suspension (5×10^4 cells/ml) were added to the upper compartment of chamber. The bottom chambers were supplemented with 500 μl F12 medium (10% FBS) and then mixed with different concentrations of Ruthenium complexes, with or without 50 ng/ml VEGF. After incubated for 24 h, the non-migrant cells at the upper face of the transwell membrane were swabbed by cottons and invaded cells were fixed with methanol for 10 minutes. After stained with Giemsa solution，pictures were taken under an Olympus inverted microscope and the statistical analysis was analyzed by manual counting. The inhibition of Percentage was expressed using untreated control cells as 100%. Three independent experiments were performed.

***In vitro* tube formation assay**

At first, Matrigel was pre-heated at 4 ℃ for 12 h and 100 μl Matrigel was added into pre-chilled 48-well plate and cultured in an incubator for half hour. HUVECs (5×10^4 cells/ml) were firstly added into the matrigel layer and then various concentrations of Ruthenium complexes or VEGF (50 ng/ml) were added. After 8-10 h, the tube formation was stained with calcein and visualized under a fluorescence microscope (IX51, Olympus). The tube length was qualified by manual counting and the inhibition percentage was expressed using untreated cells as 100%. Three independent experiments were performed.

Chorioallantoic membrane assay

The effect of NAMI-A@MSN-RGD on angiogenesis in vivo was determined by CAM (chorioallantoic membrane) assay. Briefly, fertilized eggs were incubated at 37℃ in a humidified incubator with forced air circulation. On embryonic day 6, eggs were cracked open and different concentrations of NAMI-A@MSN-RGD (50 μl/egg) were gently injected on chorioallantoic membrane. Then the embryos were incubated for another 2 days. Next, the CAM was observed under a microscope (Olympus BX 40) and photographed. VEGF was used a positive control. Effect of nano-drugs on angiogenesis was analyzed by imageproplus software and quantitatively evaluated by scoring vascular density. Six eggs per group were used in each experiment and three independent experiments were performed

Production of intracellular reactive oxygen species (ROS)

The production of ROS on HUVECs induced by NAMI-A@MSN-RGD was measured by DHE-DE assay.[54] Generally speaking, the HUVECs (10×10^5 cells/ ml) were harvested by centrifugation, then mixed with DHE-DA (10 μM) in PBS for 30 min and finally washed unstained cells by PBS. The stained cells were seeded in 96-well tissue culture plates and then added different concentrations of NAMI-A@MSN-RGD and NAMI-A

into the well. The intracellular values of ROS were immediately read on a microplate reader (SpectraMax M5, MD, USA) with the excitation and emission wavelengths at 479 and 599 nm.

The NAC blocking assay

We investigated the effect of antioxidants (NAC) on cell viability and ROS values induced by NAMI-A@MSN-RGD. The specific method was referring to previous literature.[55] For cell viability, HUVECs (10×10^4) were pretreated with NAC (10 mM) for 2 h and then incubated with NAMI-A@MSN-RGD for 24 h at different concentrations. The viability assay was investigated by MTT. For ROS levels, HUVECs were firstly treated with DHE-DA for 30 minutes and then exposed to NAC (10 mM) for 2 h at 37℃. Finally, the cells were mixed with different concentrations of NAMI-A@MSN-RGD and immediately read on a microplate reader (SpectraMax M5, MD, USA) with the excitation and emission wavelengths at 479 and 599 nm respectively.

Statistical Analysis

All experiments were carried out at least in triplicate and results were expressed as mean ± S.D. Statistical analysis was performed using SPSS statistical program version 13 (SPSS Inc., Chicago, IL). Difference between two groups was analyzed by two-tailed Student's t-test. Difference with $P < 0.05$(*) or $P < 0.01$(**) was considered statistically significant. The difference between three or more groups was analyzed by one-way ANOVA multiple comparisons.

3 Results and Discussion

Preparation and characterization of NAMI-A@MSN-RGD

At first, MSNs were synthesized as the previously reported method.[40] NAMI-A@MSN-RGD nanosystem was constructed by the scheme pictured in **Fig 1A**, and the specific methods were presented in experimental section. As shown in **Fig 1B**, the TEM images of the MSNs indicated the presence of highly dispersed and homogeneous particles with a diameter of about 60 nm. Moreover, after inspected by the Nano-particle analyzer (**Fig 1C**), the average particle size of MSNs was 100 nm, which is almost consistent with TEM. Meanwhile, loading of NAMI-A and modification of PEI-RGD didn't tempestuously change the size and dispersibility of MSNs from the **Fig 1B** and **Fig 1C**. The successfule conjugation of RGD was confirmed by a protein staningg BCA mehod and the loading ratio was 1.7μg/ml. According to the **Figure 2A**, the Zeta potential of MSNs obviously reversed after conjugation of PEI-RGD. The increasement of Zeta potential can be attributed to amino-groups on PEI-RGD. As shown in the **Fig 2B**, the maximum absorption of NAMI-A at 254 nm and 406 nm clearly shown in UV-vis spectrum of NAMI-A@MSN-RGD. In addition, the assay of N_2 adsorption-desorption was applied to investigate the physicochemical property of MSNs and NAMI-A@MSN-RGD. From the **Fig 2C 2D**, the typical nitrogen adsorption-desorption isotherm curves (IV) of MSN and NAMI-A@MSN-RGD confirmed the mesoporous material and the amounts of nitrogen adsorption at 0.8-1.0 of P/P_o increased drastically, which is attributed to the pores among the aggregated particles. Moreover, the smoothed curves of MSN at 0-0.6 P/P_o shown that MSN possessed regular mesoporous structure and the pore size curve of

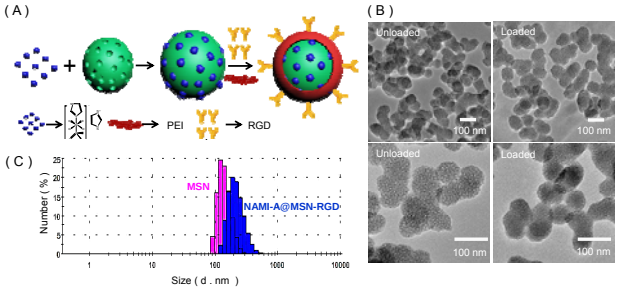

Fig. 1 Structural characterization of NAMI-A@MSN-RGD. (A) Synthetic route of NAMI-A@MSN-RGD. (B) TEM images of MSN and NAMI-A@MSN-RGD. Scale bars are 100 nm. (C) Size distribution of MSN and NAMI-A@MSN-RGD.

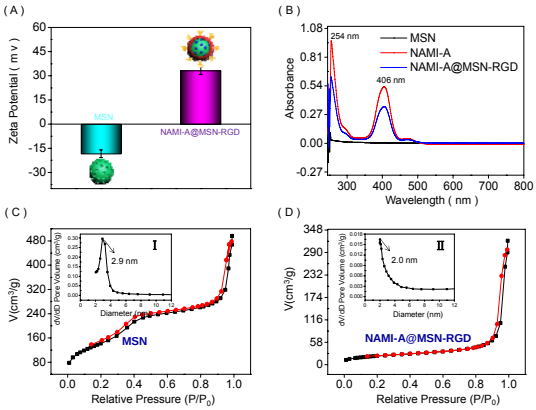

Fig. 2 Characterization of NAMI-A@MSN-RGD. (A) Zeta Potential of MSNs and NAMI-A@MSN-RGD. (B) UV-vis spectroscopy of MSNs, NAMI-A and NAMI-A@MSN-RGD. (C) a) b) N_2 adsorption–desorption isotherms of MSNs and NAMI-A@MSN-RGD (inset of Ⅰ, pore size distribution of MSNs, inset of Ⅱ, pore size distribution of NAMI-A@MSN-RGD).

MSN (inset of Ⅰ) exhibited narrow pore size (2-4 nm). After loading of NAMI-A, the pore diameter of the NAMI-A@MSN-RGD nanosystem has declined from 2.9 nm to 2.0 nm, which further demonstrated the successfully loading of NAMI-A into the MSNs. As demonstrated from the results of ICP-MS analysis, the drug loading effecience and drug loading rate of NAMI-A in MSN-RGD were found at 8.9 % and 218 $\mu g.mg^{-1}$, respectively.

Enhanced cytotoxicity and cellular uptake

Endothelial cell multiplication is a requisite step in the progress of angiogenesis. Therefore, the MTT assay was firstly employed to examine the antiproliferative activity of the newly synthesized NAMI-A@MSN-RGD. As shown in the **Fig 3A,** NAMI-A@MSN-RGD significantly enhanced the activity of NAMI-A, the IC_{50} of NAMI-A@MSN-RGD was about 12 μM to HUVECs, while NAMI-A still kept a high value of IC_{50} (459 μM). NAMI-A loaded in nanosystem is quantified by measuring Ru with ICP-MS and the following experiments were used the same quantitative approach. Moreover, we found MSNs have very low cytotoxicity even at a high concentration (**Fig 3 B).** Furthermore, **Fig 3C** also shown the noticeably different cell viability induced by NAMIA@MSN-RGD and NAMIA at the same concentration. Meanwhile, the cell viability still keep high after 72 h treatment of MSN-RGD in the same coccentration of NAMI-A@MSN-RGD, which further confimed the unique influence of NAMI-A

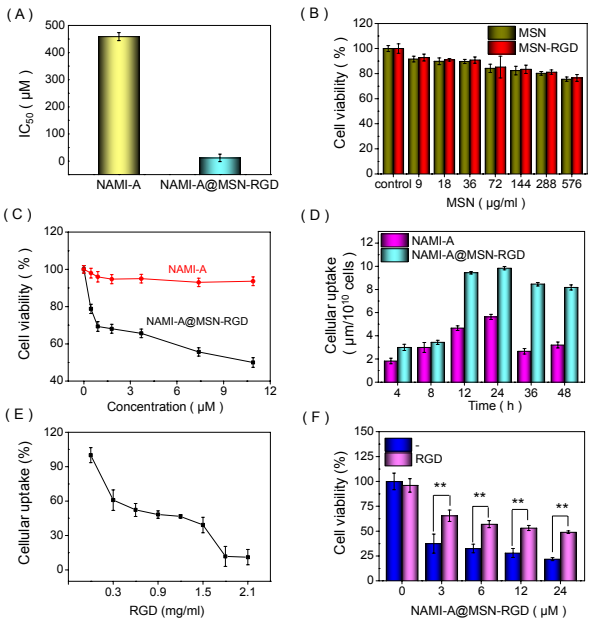

Fig. 3 (A) Cytotoxic action of NAMI-A@MSN-RGD and NAMI-A on HUVECs (2×10^4 cells/ml) after 72-h incubation. (B) *In vitro* cytotoxicity of MSN against HUVESs (2×10^4 cells / ml) in 72-h incubation. (C) The effect of NAMI-A@MSN-RGD on HUVECs (2×10^4 cells/ml) growth inhibition was investigated by 72 h MTT. (D) Quantitative cellular uptake of NAMI-A@MSN-RGD and NAMI-A in HUVECs (2×10^5 cells/ml). HUVECs are treated with NAMI-A@MSN-RGD (10 μM) and NAMI-A (10 μM) for different periods of time. The concentrations of NAMI-A was determined by ICP-MS. (E) Effect of RGD on the cellular uptake of NAMI-A@MSN-RGD was evaluated by using FITC-loaded MSN-RGD. HUVECs (2×10^5 cells/ml) were pretreated with RGD for 2 h and then exposed to FITC@MSN-RGD (2 μM) for 6 h. Cellular uptake was quantitatively operated by measuring the fluorescent intensity. (F) Effect of RGD on cell growth inhibition induced by NAMI-A@MSN-RGD. HUVECs (2×10^4 cells/ml)were firstly treated with RGD (0.25 mg/ml) for 2 h and then exposed to NAMI-A@MSN-RGD in different concentrations for 24 h. Cell viability was determined by MTT assay.

in the nanosystem. These results suggested that the application of MSNs as a drug carrier and decoration with RGD as a target agent can be an secure and effectively strategy to enhance the antiangiogenic activity of NAMI-A on HUVECs.

According to reported literature, the pharmaceutical activity of nano-based drugs is largely depended on drug delivery and cellular uptake.[29] Therefore, the quantitative analysis of cellular uptake was investigated. The same concentrations (10 μM) of NAMI-A@MSN-RGD and NAMI-A were incubated with HUVECs for different periods of time and then NAMI-A accumulated within cells were determined by ICP-MS. As shown in **Fig 3D**, the intracellular concentrations of NAMI-A@MSN-RGD was much higher than that of NAMI-A. For instance, the intracellular concentrations of NAMI-A@MSN-RGD and NAMI-A were respectively 4.7 μmol /10^{10} cells and 9.4 μmol /10^{10} cells after 12 h incubation. Furthermore, NAMI-A@MSN-RGD still kept a high concentrations (9.8μmol /10^{10} cells) while NAMI-A drastically hydrolyzed after 24 h, which hinted NAMI-A@MSN-RGD may have a longer retention time than NAMI-A within HUVECs. These results suggested that NAMI-A@MSN-RGD had a higher cellular uptake which account for the higher antiangiogenic activity than NAMI-A.

To further investigate the factors of enhanced cellular uptake and the role of RGD, we used RGD to blocking the cellular uptake of NAMI-A@MSN-RGD. As shown in the **Fig 3E**, the cellular uptake of NAMI-A@MSN-RGD was noticeably inhibited by RGD in a dose-depend manner. We guess the pretreatment of RGD would conjugate to the receptors overexpressed on HUVESs and suppressed the active target of NAMI-A@MSN-RGD. Moreover, we used additional RGD to investigate their effect on the viability of HUVECs induced by NAMI-A@MSN-RGD. The RGD can largely improve the HUVECs viability and reduce the cytotoxicity of NAMI-A@MSN-RGD (**Fig 3F**). The RGD competing assay further validated the powerful contribution of RGD in targeted transporting. In a word, the system of NAMI-A@MSN-RGD enhanced the cellular uptake through integrin receptor-mediated endocytosis, sequentially enhanced the antiangiogenic activity of NAMI-A@MSN-RGD.

Intracellular localization and drug release.

To investigate the pathway of NAMI-A@MSN-RGD entering HUVECs, we adopted fluorescence imaging technical to locating carriers. Therefore FITC labelled MSN-RGD nanoparticles were chose to simulating the intracellular track of NAMI-A@MSN-RGD. Two fluorescence probes, lyso-tracker and DAPI were used to stain lysosomes and nucleus. The **Fig 4A** revealed that the nanoparticles passed through the cell membrane in about 1 hour, aggregated in lysosomes after 2 h, and finally diffused in the entire cytoplasm, with large, lightful fluorescence observed after 8 h. According to these results, we found that NAMI-A@MSN-RGD entered HUVECs through lysosome-mediated endocytosis and cytoplasm was the main cellular target. To demonstrate the important role of endocytosis during NAMI-A@MSN-RGD entered into cells, we examined the cellular uptake and cell viability with the stimulus of various endocytosis inhibitors. From the **Fig 4B**, the internalization of NAMI-A@MSN-RGD was obviously inhibited when HUVECs pretreated with various endocytosis inhibitors. For example, Sucrose can reduce the internalization of NAMI-A@MSN-RGD from 100% to 56.5%. Furthermore, the HUVEC viability also improved along with the decrease of cellular uptake blocked by the endocytosis inhibitors (**Fig 4C**). Specifically, DOG+NaN3, Nastatin, Dynasore and Sucrose can improve the viability of HUVECs (69%) induced by NAMI-A@MSN-RGD to 83%, 81%, 74% and 71% respectively. Taken together, endocytosis through lysosomes was the important pathway of NAMI-A@MSN-RGD entering HUVEC cells. *In vitro* drug release of NAMI-A from MSN-RGD was also evaluated by coumarin-6-loaded MSN-RGD. To simulating body blood, lysosomal internal medium and intracellular environment, we chose PBS at pH 7.4, PBS at pH 5.3 and HUVEC cell lysate respectively. As shown in the **Fig 5**, coumarin-6 was laggardly released from MSN-RGD at the environment of HUVECs lysate comparing with other two environments. For instance, the accumulated release ration of coumarin-6 from MSN-RGD was about 29.8% for pH 7.4, 36.4% for pH 5.3 and 59.6% for HUVEC cell lysate after 48 h. Therefore NAMI-A@MSN-RGD nanosystem also has an excellent release performance in HUVEC cells, but not in blood circulation.

NAMI-A@MSN-RGD suppresses VEGF-induced cell migration, invasion and capillary structure formation *in vitro*.

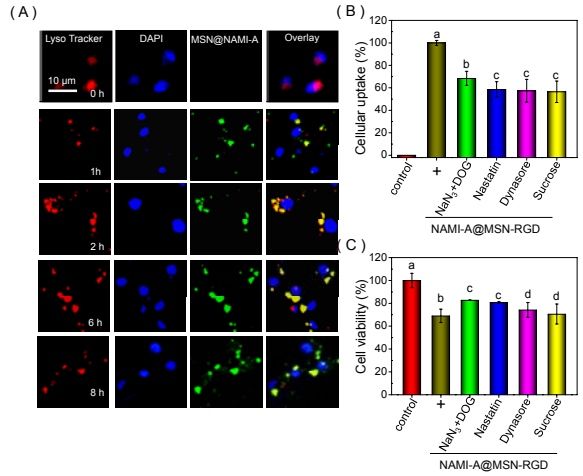

Fig. 4 (A) Intracellular trafficking of NAMI-A@MSN-RGD was investigated by FITC@MSN-RGD. HUVECs (8×10^4 cells/ml)were firstly treated with FITC@MSN-RGD (20 μM) for different periods of times and then stained with DAPI (nucleus) and Lyso tracker (lysosomes) at 37 ℃ and finally visualized under fluorescence microscope. (B) Intracellular uptake of NAMI-A@MSN-RGD in HUVECs (2×10^5 cells/ml) under different endocytosis inhibitors. Before incubation of NAMI-A@MSN-RGD, HUVECs were pretreated with specific inhibitors for different periods of times respectively. In control group, HUVECs were only treated with NAMI-A@MSN-RGD at 37 ℃. (C) Effects of various endocytosis inhibitors on cell growth inhibition induced by NAMI-A@MSN-RGD. HUVECs (2×10^4 cells/ml) were firstly treated with endocytosis inhibitors respectively for 2 h and then exposed to NAMI-A@MSN-RGD for 24 h. Cell viability was determined by MTT assay.

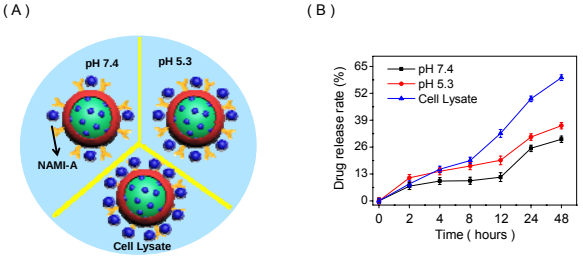

Fig. 5 (A) *In vitro* drug release of NAMI-A from NAMI-A@MSN-RGD in different pH values and cell lysate.

Angiogenesis are intensely relied on cell migration and invasion, which is also pivotal for tumor growth and metastasis.[56, 57] Therefore we adopted wound healing assay, transwell assay and tube formation assay *in vitro* to check the anti-angiogenic ability of NAMI-A@MSN-RGD. As shown in Figure 6a and 6b, the VEGF-induced enhancement of migration and invasion were effectively suppressed by NAMI-A@MSN-RGD (2 μM), while NAMI-A exhibited no obvious inhibition effect on the migration and invasion of HUVECs, even up to 200 μM. Furthermore, we employed the two-dimensional matrigel assay to examine the inhibitory effect of NAMI-A@MSN-RGD and free NAMI-A on the capillary tubule formation. After added the VEGF, elongated and strong capillary tube-like structures were formed, while obviously inhibition of capillary tube formation in a dose- way were observed after exposed to NAMI-A@MSN-RGD (**Fig 6C**). However, the formation of capillary-like structure were less

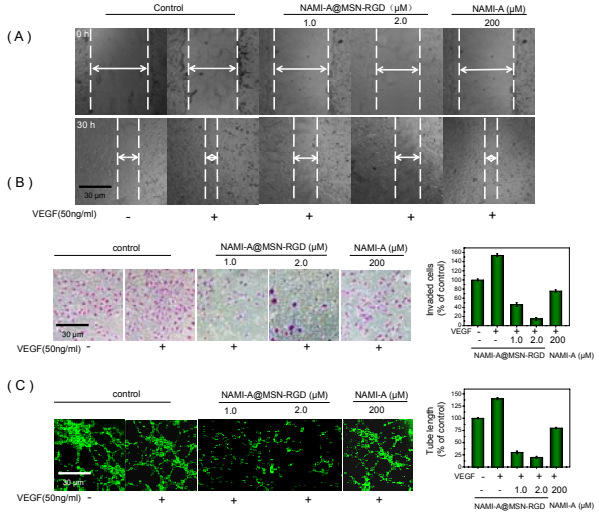

Fig. 6 (A) Anti-wounding healing assay of NAMI-A@MSN-RGD and NAMI-A on HUVEC (2×10^5 cells/ml). (B) Anti-invasion assay of NAMI-A@MSN-RGD and NAMI-A on HUVECs (5×10^4 cells/ml). (C) Anti-angiogenesis assay of NAMII-A@MSN-RGD and NAMI-A on HUVECs (5×10^4 cells/ml). The relative reduction of the width of cell healing, invaded cell numbers, capillary tube length suggested remarkable anti-metastasis effect of NAMI-A@MSN-RGD and NAMI-A. The quantitative data were analyzed by manual counting (% of control).

blocked by bare NAMI-A. These data suggested that NAMI-A@MSN-RGD possess improved and exciting antiangiogenic activity compare to NAMI-A.

NAMI-A@MSN-RGD suppress VEGF-induced angiogenesis in CAM model.

The chorioallantoic membranes of the fertilized eggs have profuse branching of vessels and they are fairly sensitive to antiangiogenic drugs. Therefore the ability of NAMI-A@MSN-RGD to inhibit angiogenesis *in vivo* was performed using chick embryo chorioallantoic membrane (CAM) angiogenesis assay. As illustrated in **Fig 7**, the CAM neovascularization was significantly enhanced by VEGF, but obviously suppressed by NAMI-A@MSN-RGD (10 μM). Similar to the inhibition effect on endothelial proliferation *in vitro*, NAMI-A@MSN-RGD exhibits a stronger inhibition on CAM angiogenesis than NAMI-A. In sum, these results certified that our decoration of NAMI-A with MSN and RGD was an effective and valuable exploration.

Apoptosis induced by NAMI-A@MSN-RGD HUVEC cells.

Induction of endothelial cell apoptosis is an effective way to inhibit angiogenesis.[57] Therefore, PI-flow analysis was employed to measure the cell cycle and apoptosis after treatment with synthesized drugs. As shown in the **Fig 8**, NAMI-A@MSN-RGD can induce apoptosis of HUVECs in a dose-dependent way, as reflected by the increase in Sub-G1 peaks. For example, the cells in Sub-G1 phase were distinctly increased to 20 %, 45.2 % and 67.4 % respectively after 72-h incubation with 1.5, 3.0 and 6.0 μM NAMI-A@MSN-RGD. By contrast, the activity of NAMI-A was much lower than NAMI-A@MSN-RGD even at a very high concentration. These results indicated that NAMI-A@MSN-RGD inhibit angiogenesis were mainly through induction of apoptosis.

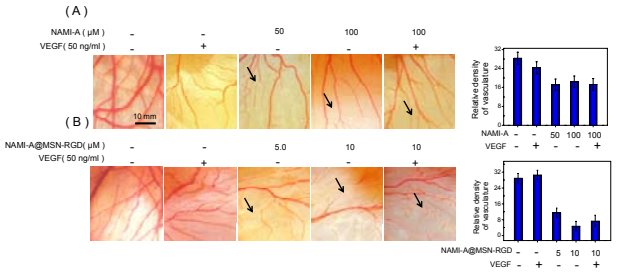

Fig. 7 The anti-angiogenic activity of NAMI-A@MSN-RGD and NAMI-A in CAM model. NAMI-A@MSN-RGD (10 μM) induced obvious inhibition of vasculature architecture even the adding of VEGF (50 ng/ml) compare to the NAMI-A. The mean microvessel density was qualified by IPP (Image proplus).

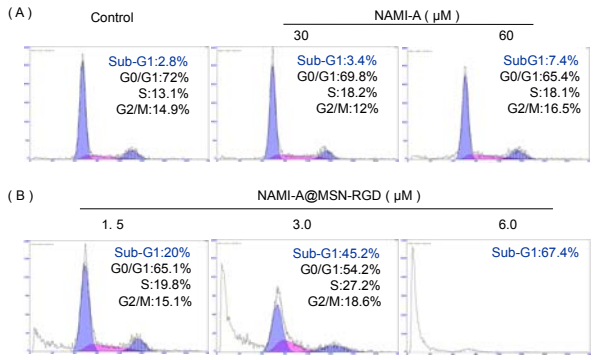

Fig. 8 Flow cytometric analysis of NAMI-A@MSN-RGD on HUVECs for 72 h.

NAMI-A@MSN-RGD trigged ROS-mediated DNA damage

ROS (Reactive oxygen species) is a category of important and unique chemical substances that adjust the signal transduction trigged by various cancer drugs, such as platinum complexes and ruthenium complexes.[58, 59] Most of anticarcinogens cause cancer cell apoptosis by ROS up-regulation.[46] Therefore, we adopted DHE-fluorescence method to measure the levels of ROS in HUVECs after exposed to the NAMI-A@MSN-RGD and NAMI-A in different periods of times. As shown in **Fig 9A**, HUVECs exhibited prodigious intensity of fluorescence after the treatment of NAMI-A@MSN-RGD. However, NAMI-A shown very weak fluorescence values, which is consistent with their anti-angiogenesis activity. The single carriers of MSNs also showed a weak ascending trend of ROS from the **Fig 9A**. For instance, NAMI-A@MSN-RGD can produced a high ROS level (173.5%) while NAMI-A only shown a low ROS level (103%) after 55 minutes. Moreover, the fluorescence image of ROS directly shown NAMI-A@MSN-RGD produce a high ROS level in 120 minutes from the **Fig 9B**. To prove ROS plays an important role in NAMI-A@MSN-RGD elicited cell death, we further used N-acetylcysteine (NAC 10 mM), a thiol-reducing antioxidant, to block the overproduction of ROS. From the **Fig 9C** and **9D**, NAC distinctly suppressed the generation of ROS and reduced the cytotoxicity of NAM-A@MSN-RGD. For instance, NAC (10 mM) can reduce the ROS production in HUVECs treated with1.6 μM NAMI-A@MSN-RGD from 178% to 122% and improve the cell viability from 55% to 66%. Taken these results together, we

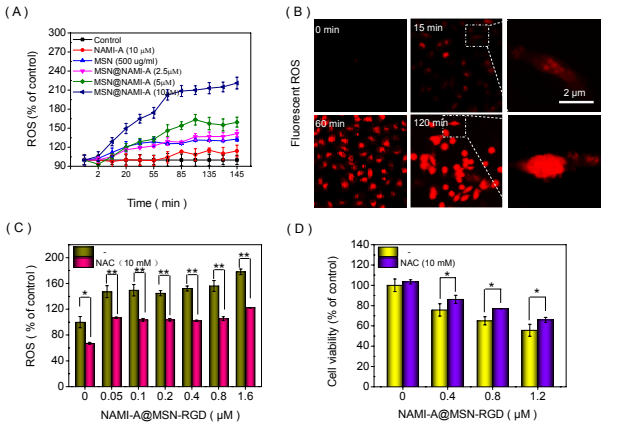

Fig. 9 (A) The up-regulation of ROS in HUVECs (10×10^5 cells/ml) exposed to NAMI-A@MSN-RGD. ROS values measured in a microplate reader after exposed to NAMI-A@MSN-RGD at indicated concentrations and expressed as relative fluorescence intensity. (B) The fluorescent ROS in HUVECs (10×10^5 cells/ml) after exposed to NAMI-A@MSN-RGD (0.25 μM) in different periods of time. (C) The antioxidants NAC (10 mM) obviously reduce the production of ROS (10×10^5 cells/ml) induced by NAMI-A@MSN-RGD. HUVECs were firstly treated with NAC (10 mM) for 2 h and then exposed to NAMI-A@MSN-RGD at indicated concentrations. (D) The antioxidants NAC obviously inhibited the cell growth induced by NAMI-A@MSN-RGD. HUVECs (2×10^4 cells/ml) were treated with RGD (10 mM) for 2 h and then exposed to NAMI-A@MSN-RGD for 24 h. Cell viability was determined by MTT assay.

confirmed that ROS was an important signaling pathway in HUVECs apoptosis induced by NAMI-A@MSN-RGD.

4 Conclusions

In this study, an effective angiogenesis-targeted transport system was successfully constructed and characterized. This nanosystem used RGD-peptide modified MSNs loaded a well-known Ru complex NAMI-A to enhance the antiangiogenesis efficacy. The NAMI-A@MSN-RGD obviously inhibits cell proliferation and VEGF-provoked migration, invasion and capillary structure formation in endothelial cells. Moreover, the antiangiogenic effect of NAMI-A@MSN-RGD in vivo was investigated by the CAM assay and the chick embryo neovascularization was clearly suppressed. Furthermore, the anti-angiogenic activity of NAMI-A@MSN-RGD was much higher than individual NAMI-A after the decoration of MSNs and RGD. Specially, the surface decoration of RGD effectively promoted the cellular uptake of NAMI-A@MSN-RGD through receptor-mediated endocytosis. Preliminary mechanism investigation indicates NAMI-A@MSNs-RGD inhibit angiogenesis through induction of ROS-triggered apoptosis in HUVECs. Our results confirmed that the strategy to use RGD-peptide functionalized MSNs as carriers of NAMI-A is an effectively way to enhance caner-targeted antiangiogenesis.

Acknowledgements

This work was supported by National High Technology Research and Development Program of China (863 Program, SS2014AA020538), Science Foundation for Distinguished Young Scholars (S2013050014667) of Guangdong Province, Foundation for High-level Talents in Higher Education of

Guangdong, Natural Science Foundation of China, Research Fund for the Doctoral Program of Higher Education of China (20114401110004), Shenzhen Basic Research Grant (JCYJ20130401152508660) and YangFan Innovative & Entepreneurial Research Team Project (201312H05).

Notes and references

Department of Chemistry, Jinan University, Guangzhou 510632, China. Fax: +86 20 85221263; Tel: +86 20-85225962;E-mail: tchentf@jnu.edu.cn

† Electronic Supplementary Information (ESI) available: [details of any supplementary information available should be included here]. See DOI: 10.1039/b000000x/

1. S. M. Weis and D. A. Cheresh, *Nat. Med.*, 2011, **17**, 1359-1370.
2. P. Carmeliet and R. K. Jain, *Nature*, 2011, **473**, 298-307.
3. M. Kowanetz and N. Ferrara, *Clin. Cancer Res.*, 2006, **12**, 5018-5022.
4. A. S. Chi, A. D. Norden and P. Y. Wen, *NeuroTherapeutics*, 2009, **6**, 513-526.
5. S. M. Weis and D. A. Cheresh, *Nature*, 2005, **437**, 497-504.
6. J. A. García-Vilas, A. R. Quesada and M. Á. Medina, *J. Agric. Food Chem.*, 2013, **61**, 4063-4071.
7. A. Muth, V. Pandey, N. Kaur, M. Wason, C. Baker, X. Han, T. R. Johnson, D. A. Altomare and O. t. Phanstiel, *J. Med. Chem.*, 2014, **57**, 4023-4034.
8. M. J. Clarke, *Coord. Chem. Rev.*, 2002, **232**, 69-93.
9. Q. A. de Paula, R. W. D. Franco, M. B. Ribeiro, J. Ellena, E. E. Castellano, O. R. Nascimento and A. A. Batista, *J. Mol. Struct.*, 2008, **891**, 64-74.
10. P. J. Dyson and G. Sava, *Dalton Trans.*, 2006, 1929-1933.
11. M. A. Jakupec, M. Galanski, V. B. Arion, C. G. Hartinger and B. K. Keppler, *Dalton Trans.*, 2008, 183-194.
12. D. C. Kennedy, B. O. Patrick and B. R. James, *Can. J. Chem.*, 2011, **89**, 948-958.
13. A. Levina, A. Mitra and P. A. Lay, *Metallomics*, 2009, **1**, 458-470.
14. J. M. Rademaker-Lakhai, D. van den Bongard, D. Pluim, J. H. Beijnen and J. H. M. Schellens, *Clin. Cancer Res.*, 2004, **10**, 3717-3727.
15. F. Lentz, A. Drescher, A. Lindauer, M. Henke, R. A. Hilger, C. G. Hartinger, M. E. Scheulen, C. Dittrich, B. K. Keppler, U. Jaehde and C. E. S. A. D. Re, *Anti-Cancer Drugs*, 2009, **20**, 97-103.
16. C. G. Hartinger, S. Zorbas-Seifried, M. A. Jakupec, B. Kynast, H. Zorbas and B. K. Keppler, *J. Inorg. Biochem.*, 2006, **100**, 891-904.
17. C. G. Hartinger, M. A. Jakupec, S. Zorbas-Seifried, M. Groessl, A. Egger, W. Berger, H. Zorbas, P. J. Dyson and B. K. Keppler, *Chem. Biodiversity*, 2008, **5**, 2140-2155.
18. J. M. Rademaker-Lakhai, D. van den Bongard, D. Pluim, J. H. Beijnen and J. H. Schellens, *Clin. Cancer Res.*, 2004, **10**, 3717-3727.
19. M. M. Henke, H. Richly, A. Drescher, M. Grubert, D. Alex, D. Thyssen, U. Jaehde, M. E. Scheulen and R. A. Hilger, *Int. J. Clin. Pharmacol. Ther.*, 2009, **47**, 58-60.
20. A. Levina, A. Mitra and P. A. Lay, *Metallomics*, 2009, **1**, 458-470.
21. D. Chatterjee, A. Mitra, A. Levina and P. A. Lay, *Chem. Commun.*, 2008, 2864-2866.
22. S. M. Nie, Y. Xing, G. J. Kim and J. W. Simons, *Annu. Rev. Biomed. Eng.*, 2007, **9**, 257-288.
23. M. Shi, K. Ho, A. Keating and M. S. Shoichet, *Adv. Funct. Mater.*, 2009, **19**, 1689-1696.
24. P. Koley and A. Pramanik, *Adv. Funct. Mater.*, 2011, **21**, 4126-4136.
25. C. Minelli, S. B. Lowe and M. M. Stevens, *Small*, 2010, **6**, 2336-2357.
26. C. R. Steven, G. A. Busby, C. Mather, B. Tariq, M. L. Briuglia, D. A. Lamprou, A. J. Urquhart, M. H. Grant and S. V. Patwardhan, *J. Mater. Chem. B*, 2014, **2**, 5028-5042.
27. N. Prabhakar, T. Nareoja, E. von Haartman, D. S. Karaman, H. Jiang, S. Koho, T. A. Dolenko, P. E. Hanninen, D. I. Vlasov, V. G. Ralchenko, S. Hosomi, Vlasov, II, C. Sahlgren and J. M. Rosenholm, *Nanoscale*, 2013, **5**, 3713-3722.
28. G. Zhang, M. Yang, D. Cai, K. Zheng, X. Zhang, L. Wu and Z. Wu, *ACS Appl. Mater. Interfaces*, 2014, **6**, 8042-8047.
29. D. Peer, J. M. Karp, S. Hong, O. C. FaroKHzad, R. Margalit and R. Langer, *Nat. Nanotechnol.*, 2007, **2**, 751-760.
30. J. J. Shi, A. R. Votruba, O. C. Farokhzad and R. Langer, *Nano Lett.*, 2010, **10**, 3223-3230.
31. V. Lebret, L. Raehm, J. O. Durand, M. Smaihi, M. H. V. Werts, M. Blanchard-Desce, D. Methy-Gonnod and C. Dubernet, *J. Biomed. Nanotechnol.*, 2010, **6**, 176-180.
32. S. Hudson, J. Cooney and E. Magner, *Angew. Chem., Int. Ed.*, 2008, **47**, 8582-8594.
33. J. L. Vivero-Escoto, I. I. Slowing, B. G. Trewyn and V. S. Y. Lin, *Small*, 2010, **6**, 1952-1967.
34. M. Vallet-Regi, F. Balas and D. Arcos, *Angew. Chem., Int. Ed.*, 2007, **46**, 7548-7558.
35. E. Katz and I. Willner, *Angew. Chem., Int. Ed.*, 2004, **43**, 6042-6108.
36. R. Hao, R. J. Xing, Z. C. Xu, Y. L. Hou, S. Gao and S. H. Sun, *Adv. Mater.*, 2010, **22**, 2729-2742.
37. S. Goel, F. Chen, H. Hong, H. F. Valdovinos, R. Hernandez, S. Shi, T. E. Barnhart and W. Cai, *ACS Appl. Mater. Interfaces*, 2014, **6**, 21677-21685.
38. X. J. Liu, F. F. Fu, K. B. Xu, R. J. Zou, J. M. Yang, Q. Wang, Q. Liu, Z. Y. Xiao and J. Q. Hu, *J. Mater. Chem. B*, 2014, **2**, 5358-5367.
39. K. K. P. Mitchell, S. Sandoval, M. J. Cortes-Mateos, J. G. Alfaro, A. C. Kummel and W. C. Trogler, *J. Mater. Chem. B*, 2014, **2**, 8017-8025.
40. L. M. Pan, Q. J. He, J. N. Liu, Y. Chen, M. Ma, L. L. Zhang and J. L. Shi, *J. Am. Chem. Soc.*, 2012, **134**, 5722-5725.
41. D. P. Ferris, J. Lu, C. Gothard, R. Yanes, C. R. Thomas, J. C. Olsen, J. F. Stoddart, F. Tamanoi and J. I. Zink, *Small*, 2011, **7**, 1816-1826.
42. T. Inoue, P. G. Cavanaugh, P. A. Steck, N. Brunner and G. L. Nicolson, *J. Cell. Physiol.*, 1993, **156**, 212-217.
43. H. N. Keer, J. M. Kozlowski, Y. C. Tsai, C. Lee, R. N. McEwan and J. T. Grayhack, *J. Urol.*, 1990, **143**, 381-385.
44. E. Ryschich, G. Huszty, H. P. Knaebel, M. Hartel, M. W. Buchler and J. Schmidt, *Eur. J. Cancer*, 2004, **40**, 1418-1422.

45. L. He, T. Chen, Y. You, H. Hu, W. Zheng, W. L. Kwong, T. Zou and C. M. Che, *Angew. Chem.*, 2014, **53**, 12532-12536.
46. K. Apel and H. Hirt, *Annu. Rev. Plant Biol.*, 2004, **55**, 373-399.
47. B. Yu, X. Li, W. Zheng, Y. Feng, Y.-S. Wong and T. Chen, *J. Mater. Chem. B*, 2014, **2**, 5409.
48. T. Chen and Y. S. Wong, *Biomed. Pharmacother.*, 2009, **63**, 105-113.
49. W. Jiang, Y. Fu, F. Yang, Y. Yang, T. Liu, W. Zheng, L. Zeng and T. Chen, *ACS Appl. Mater. Interfaces*, 2014, **6**, 13738-13748.
50. Y. Huang, Y. Luo, W. Zheng and T. Chen, *ACS Appl. Mater. Interfaces*, 2014, **6**, 19217-19228.
51. L. M. Wilhelmsson, F. Westerlund, P. Lincoln and B. Norden, *J. Am. Chem. Soc.*, 2002, **124**, 12092-12093.
52. W. Liu, X. L. Li, Y. S. Wong, W. J. Zheng, Y. B. Zhang, W. Q. Cao and T. F. Chen, *Acs Nano*, 2012, **6**, 6578-6591.
53. Y. Huang, L. He, W. Liu, C. Fan, W. Zheng, Y. S. Wong and T. Chen, *Biomaterials*, 2013, **34**, 7106-7116.
54. T. F. Chen and Y. S. Wong, *Int. J. Biochem. Cell Biol.*, 2009, **41**, 666-676.
55. C. Tan, S. Lai, S. Wu, S. Hu, L. Zhou, Y. Chen, M. Wang, Y. Zhu, W. Lian, W. Peng, L. Ji and A. Xu, *J. Med. Chem.*, 2010, **53**, 7613-7624.
56. A. G. Tkachenko, H. Xie, D. Coleman, W. Glomm, J. Ryan, M. F. Anderson, S. Franzen and D. L. Feldheim, *J. Am. Chem. Soc.*, 2003, **125**, 4700-4701.
57. H. L. Sun, A. C. Tsai, S. L. Pan, Q. Q. Ding, H. Yamaguchi, C. N. Lin, M. C. Hung and C. M. Teng, *Clin. Cancer Res.*, 2009, **15**, 4904-4914.
58. L. L. Li, Y. S. Wong, T. F. Chen, C. D. Fan and W. J. Zheng, *Dalton Trans.*, 2012, **41**, 1138-1141.
59. H. Pelicano, D. Carney and P. Huang, *Drug Resist. Updates*, 2004, **7**, 97-110.

TABLE OF CONTENT

Herein we demonstrate the use of RGD-modified MSNs as a vehicle of anticancer drugs to achieve enhanced antiangiogenic activity.